Pseudo-Random Channel Shuffling Time-Division Multiplexing of Ultrasound Echoes in Ultrasound Imaging Integrated Circuits

Dias, Diogo; Goes, João; Desmarais, Samuel; Costa, Tiago M.L.

DOI
10.1109/IUS62464.2025.11201729

Publication date
2025

Document Version
Final published version

Published in
2025 IEEE International Ultrasonics Symposium, IUS 2025

Pseudo-Random Channel Shuffling Time-Division Multiplexing of Ultrasound Echoes in Ultrasound Imaging Integrated Circuits

Diogo Dias, João Goes
Dept. of Electrical and Computer Eng.
LASI, UNINOVA-CTS
Monte de Caparica, Portugal
das.dias@campus.fct.unl.pt

Samuel Desmarais, Tiago M. L. Costa
Bioelectronics Group, Microelectronics Dpt.
EEMCS-Delft University of Technology
Delft, The Netherlands

2025 IEEE International Ultrasonics Symposium (IUS) | 979-8-3315-2332-9/25/$31.00 ©2025 IEEE | DOI: 10.1109/IUS62464.2025.11201729

***Abstract*—Next generation wearable/implantable ultrasound imaging systems demand ultra-compact, power-efficient analog front-end circuits enabling high-resolution, high frame-rate multimodal imaging. Individual RF channel access allows for the use of state-of-the-art imaging methods such as synthetic aperture imaging, plane-wave compounding and adaptive beamforming, while remaining crucial for auto-calibration of sparse transducer arrays. Time-division multiplexing-based (TDM) architectures have been widely deployed to enable individual RF channel access, but impose severe trade-offs between power and silicon area for imaging quality and contrast. This work introduces a *pseudo-random channel-shuffling* TDM (PRCS-TDM) technique, emulating a non-uniform sampling-rate for each RF channel. Results show PRCS-TDM improves B-mode contrast-to-noise ratio (CNR) in anechoic regions up to a 2× increase compared to conventional TDM, achieving a 3.2 dB CNR increase for channel compression ratios greater than 8.**

***Index Terms*—Analog Front-End, Ultrasound Imaging, Ultrasound Stimulation, ASICs, Compressive Sensing**

I. Introduction

Wearable ultrasound (US) imaging systems demand ultra-compact, power-efficient analog front-end (AFE) circuits enabling high-resolution 2D/3D imaging [1], [2]. Since image quality is directly proportional to the total number of transducers and their density in a 2D array configuration, increasing imaging quality often demands the number of recording channels to exceed the many hundreds and even thousands. This in turn leads to a bottleneck in the number of cables required to interface the imaging ASIC to external electronics. Cable-count reduction in catheter-based ultrasound (US) imaging (USI) systems was the primary motivation for the development of image-quality preserving multiplexing AFEs [3]. However, the sheer volume of ultrasound data retrieved from the AFE in 2D and 3D low power USI systems requires integrated architectures capable of compressing output channels in both aperture and time domains [2]. Moreover, access to individual RF data (Fig.1 a) enables the use of imaging algorithms beyond fixed-aperture (analog) beamforming, such as synthetic aperture imaging, plane-wave compounding, adaptive beamforming, while facilitating the integration of advanced digital processing, enabling auto-calibration of sparse transducer arrays, and artificial intelligence within the medical device [4], [5]. Sub-array beamforming (μBF) AFE architectures have become the golden-standard for ASIC architectures aiming to achieve substantial RF channel compression while optimizing obtained image quality, performing on-chip noise-averaging

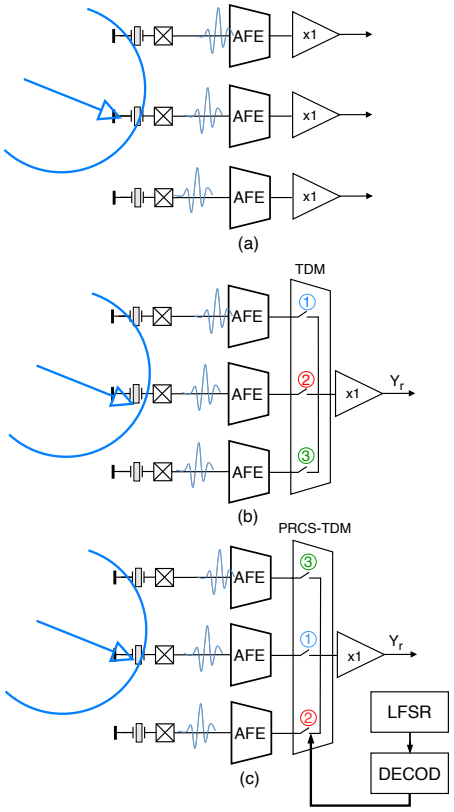

Fig. 1. Simulated AFE architectures using a) fully-addressed 1D transducer array, b) TDM indexing, c) and the proposed PRCS-TDM scheme.

This work has been supported by Portuguese National Science and Technology Foundation (FCT) under the PhD grant UI/BD/153604/2022, and CTS multiannual funding program CTS/00066.

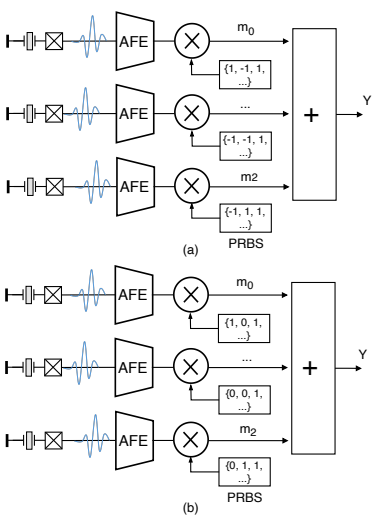

Fig. 2. Compressive multiplexing AFE based on a) bipolar PRBS aperture-domain multiplexing, and b) unipolar PRBS time-domain multiplexing [11], [14].

in both the electrical and acoustic domains [3], [6]. However, μBF architectures do not preserve the information of the individual RF channel, limiting imaging modalities to scan-line imaging and constraining the frame-rate of integrated imaging devices to 2000 frames/s [6]. As an alternative, time-division multiplexing (TDM) (Fig.1 b) has been widely adopted for output channel and cable count reduction, however, it imposes severe trade-offs between power and silicon area against imaging quality [7], [8]. Alternatively, the compatibility of spread-spectrum multiplexing techniques with compressive sensing and non-uniform sampling of US echoes [9]–[11] offers a promising path for reliable on-chip compression in time and aperture domains of individual RF channel data [4].

This work presents the study of an AFE architecture with an area-efficient *pseudo-random channel-shuffling* TDM (PRCS-TDM) technique, leveraging the random ordering of RF channel TDM access in order to emulate a unipolar pseudo-random bit-stream (PRBS) (Fig.1 c) -based non-uniform sampling-rate for each RF channel - aiming to improve imaging quality while maintaining similar power and die area figures relative to TDM. This paper is organized as follows: Sec. II introduces the US echo model and the theoretical background supporting the remainder of the work, Sec.III describes the derivation of the method from the description of TDM as signal reconstruction problem, Sec.IV describes the simulation setup and reconstruction and imaging quality evaluation framework allowing for the results descussion and drawn conclusions regarding the competitiveness of the method against conventional TDM in Secs.V and VI, respectively.

II. Compressive Multiplexing and Non-Uniform Sampling of Band-Limited Signals

US echo signals $m(t)$ can be modeled through the pulse-stream model (1), representing echoes as a superposition of band-limited gaussian-modulated cosine basis-kernels $v(t)$ [9], [10]. A convolutional basis matrix $\mathbf{V}$, defined column-wise by time-shifted versions of $v(t)$, facilitates sparse representation and processing of each RF channel $m_j(t) = \sum_{k=1}^{K} m_k \cdot v(t - t_R^{k,j})$, resulting in a $m_j \in \mathcal{M}_{N,1}(\Re)$ vector obtained at a sampling rate F_S, represented through

$$m_j = \mathbf{V} \times \hat{m}_j + \epsilon_j, \ \|m\|_0 \leq K \tag{1}$$

where $\epsilon_j \in \mathcal{M}_{N,1}(\Re)$ is the basis-kernel projection error, allowing most of the coefficients of $\hat{m}_j$ to be null, except for those at true scatterer locations [9], [13]. Projecting the US echoes into a convolution kernel of time-sparse signals (1) results in band-limited signals that are sparse in both frequency and time domains, an US echo model highly compatible with compressive sensing (CS) algorithms [12], [14].

CS is crucial for managing the substantial data throughput from US probes in diagnostics, reducing hardware and sampling rate requirements [13], [14]. Chipping PRBS sequences must be orthogonal to ensure accurate recovery of modulated signals, minimize cross-correlation across multiplexed channels, and maximize auto-correlation towards 1 ($(\mathbf{P} \odot \mathbf{M})^T (\mathbf{P} \odot \mathbf{M}) \ \rightarrow \ \mathbf{I_J}$). Data compression can be achieved in the aperture domain, using bipolar PRBS $p_j(t) = \{-1, 1\}$ to modulate multiple information channels (Fig. 2 a) [10], [11], and in the time domain, using unipolar PRBS $p_j(t) = \{0, 1\}$ for non-uniform and sub-Nyquist sampling of individual RF channels (Fig. 2 b) [12].

The compressive multiplexer (CMUX) [11] exemplifies an aperture-multiplexing architecture, enabling individual RF channel spectrum-spreading through bipolar PRBS, and leveraging passive noise averaging and code orthogonality for signal reconstruction, as observed in the Butterfly IQ hand-held probe [4]. CMUX allows the quantizer to operate at the same rate as the PRBS modulator and eliminates the need for an integrator, making it more attractive for hardware implementation when compared to the random modulator (RD) [11]. The output of any architecture employing CS can be described as in (2)

$$\mathbf{Y} = (\mathbf{P} \odot \mathbf{M}) \ \mathbf{A} \tag{2}$$

where $\mathbf{Y} \in \mathcal{M}(\Re)_{N_S,R}$ are the column-wise output signals, $\mathbf{P} \in \mathcal{M}(\Re)_{N_S,J}$ are the column-wise PRBS modulating each individual input RF channel, $\mathbf{M} \in \mathcal{M}(\Re)_{N_S,J}$ is the column-wise samples of each multiplexed RF channel, and $\mathbf{A} \in \mathcal{M}(\Re)_{J,R}$ is the summation matrix stating which of the J input RF channels are modulated and superposed together [10], [11]. The vector basis pursuit problem in (3) facilitates sample matrix reconstruction using L1-regularization penalty (λ_j) to promote sparsity in $\hat{\mathbf{M}}$, for efficient denoising and de-correlation across multiplexed channels when there exists coherent interference between samples.

$$\hat{\mathbf{M}} \approx arg \ \min_{\mathbf{M}} \ \frac{1}{2} \left\| \mathbf{Y} - (\mathbf{P} \odot (\mathbf{V}\hat{\mathbf{M}}))\mathbf{A} \right\|_F^2 + \sum^{J} \lambda_j \left\| \hat{\mathbf{M}}_{:,j} \right\|_1 \tag{3}$$

III. Pseudo-Random Channel Shuffling Time-Division Multiplexing

A. Impact of PRBS Codes in Recovered Energy

In equal-probability bipolar modulation, channel samples are collected with values $\{-A, A\}$, yielding an average energy per sample of $\langle E \rangle = A^2$, while unipolar streams yield an average energy of $\langle E \rangle = \frac{1}{2}A^2$ for samples within $\{0, A\}$. Bipolar chipping sequences demand a dedicated summation block, requiring additional active OTA-based blocks for precise summation operation [4], [11]. Moreover, iterative reconstruction approaches to estimate $\hat{\mathbf{M}}$ are required, leading to additional required memory and computational complexity for solving (3), consequently reducing the frame-rate of imaging algorithms.

B. Time-Division Multiplexing as a Compressive-Sensing Reconstruction Problem

Despite lower energy and reduced denoising potential, unipolar bit-streams correspond directly to system-level sampling events, allowing compact power-efficient on-chip implementation, and facilitating integration into existing systems using TDM in synthetic-aperture USI ASICs. Re-casting TDM as a reconstruction problem in (2) reveals that the sampling chipping code matrix $\mathbf{P}_{TDM} = \mathbf{I}_C$ for each subset of compressed channels C within total RF channels J ($C \in J$) is a time-domain collision-free orthogonal unipolar code, eliminating the need of convex-optimization upon channel reconstruction. In this case, the $\mathbf{V_{pe}}$ convolutional kernel implements an interpolating filter on the sampled measurement matrix $\mathbf{P_{TDM}} \odot \hat{\mathbf{M}}$ (4).

$$\hat{\mathbf{M}} \approx \mathbf{V}(\mathbf{P}_{(\mathbf{PRCS-})\mathbf{TDM}} \odot (\mathbf{Y}\mathbf{A}^T)) \tag{4}$$

While TDM uses a Johnson counter for interleaved selection of input RF channels connected to the AFE output (Fig. 1b), a C-bit output linear feedback shift register (LFSR) can (pseudo-)randomly select the index of the 2^C multiplexed channels, incorporating a $C \rightarrow 2^C -$ bit decoder for individual channel selection (Fig.1c). PRCS-TDM emulates a non-uniform sampling PRBS by swapping the columns of $\mathbf{P}_{TDM}$ randomly, generating $\mathbf{P}_{PRCS-TDM}$. A $C = 3$ example is shown in (1 d). Similarly to TDM, reconstructing RF channels multiplexed using PRCS-TDM falls down to solving (4).

IV. Simulation Setup and Evaluation Framework

A. Simulation Setup

US RF simulation data was collected using the PyMUST scatterer-based simulator [16], to simulate the proposed PRCS-TDM topology. Synthetic 2D B-mode US images were generated from steered plane wave transmission and compounded from beamformed time-gain-compensated low-pass-filtered RF echo envelopes [17]. The 2D computational domain featured a grid of 258×258 along the azimuthal (x) and longitudinal (z) directions, with an imaging azimuth of 50 mm and a longitudinal range of 0 to 75 mm (1.5× the azimuth range). A center frequency of 4.0 MHz and a relative fractional bandwidth of 100% were used. The sampling frequency was initially set to the Nyquist rate $F_S = 4 \times f_c$. Transducer parameters are summarized in Table I.

TABLE I
Linear array transducer parameters used in the simulation.

Parameter	Symbol	Value
Number of elements	J	32
Center frequency	f_c	4.0 MHz
Element width	w	180 μm
Kerf (inter-element spacing)	k	20 μm
Pitch (center-to-center spacing)	p	200 μm
Element height	h	180 μm
Bandwidth	$B_{[\%]}$	100%
Sampling Frequency	F_S	16 MHz

Scatterers featuring random reflectivity coefficients $\Gamma \in \Re[0, 1]$ were placed randomly within the grid, for emulation of acoustic background noise. A divergent wave transmission - increasing the angular field-of-view (FOV_θ) - results from the limited F-number of the 1D linear array ($F\# = F_D/(J\ p - k(J-1)) \approx 0.15$), with the natural focal-depth $F_D = (J\ p - k(J-1))\ h/\pi\lambda \approx 0.9$ mm resulting from the limited aperture of the 1D linear array [17]. The required number of steered planar-wave transmissions N_{PWT} to obtain a similar imaging quality to scan-line imaging translates to $N_{PWT} = (J\ p - k(J-1))/\lambda F\# \approx 101$, at a $FOV_\theta \approx \pm 30°$ [17]. However, to reduce long simulation times, N_{PWT} was empirically set to 17, allowing for sufficient image quality to conduct our study.

B. Evaluation Framework

A fully addressed architecture (Fig.1 a) was used to obtain a reference B-mode US image (Fig. 4 c). Testing phantoms with *anechoic* ($\Gamma = 0$) and *hyperechoic* ($\Gamma = 1$) circular regions of varying diameters between 2 mm and 9 mm (Fig. 4 c) [18] were used to evaluate image quality. RF channel compression ratios of 4:1 and 8:1 using TDM (Fig. 1 b) and the proposed PRCS-TDM (Fig. 1 c) architectures were compared against the reference image. Measurement metrics included: a) classical contrast-to-noise ratio (CNR) defined as $\text{CNR} = |\mu_{ROI} - \mu_B|/\sqrt{\sigma^2_{ROI} + \sigma^2_B}$, where μ_{ROI} and μ_B are the mean pixel intensities of the regions of interest (ROI) and the background, respectively, and σ_1^2 and σ_2^2 are their corresponding variances; b) generalized CNR (gCNR) given by $gCNR = S^{-1/(S-1)} - S^{-S/(S-1)}$, measuring the perceptibility of anechoic (a-gCNR) and hyperechoic (h-gCNR) regions in a B-mode US image, with S derived from CNR using the relation $\text{CNR} = |S-1|/\sqrt{S^2+1}$ [19]; and c) structural similarity index measurement (SSIM), comparing contrast, illumination, and overall structures between a reference image x and a distorted image y, defined as $\text{SSIM}(x, y) = \frac{(2\mu_x\mu_y)(2\sigma_{xy})}{(\mu_x^2+\mu_y^2)(\sigma_x^2+\sigma_y^2)}$ [20].

V. Results and Discussion

The choice of PRBS for random channel indexing was observed to significantly impact RF channel reconstruction. Lack of sampling events and acquisition for long periods significantly constrains the measured energy of a signal,

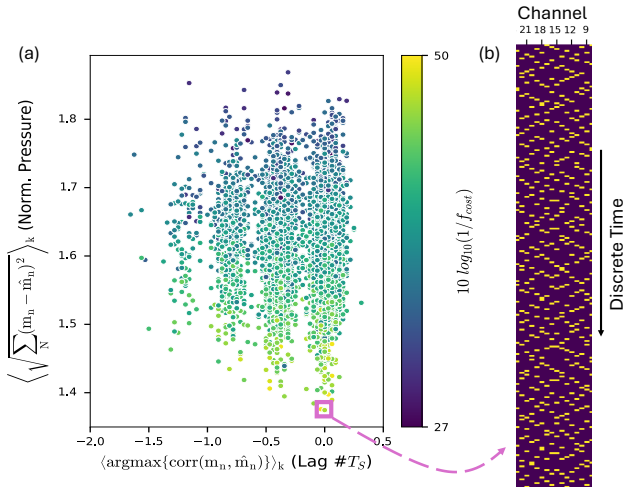

Fig. 3. a) Simulated epochs in search of optimal PRCS-TDM indexing sequences, b) Found (locally) optimal PRBS sequence.

degrading image quality. Consequently, optimal code sequences were searched through a broad random-sampling exploration of PRBS chipping codes in each epoch (Fig. 3a), arriving at the (locally) optimal chipping sequences shown in Fig. 3b. The total Cartesian distance $D_m = \|m_j - \hat{m}_j\|_2 = \sqrt{\sum_n^{N_s}(m_j(n) - \hat{m}_j(n))^2}$ and total lag $L_m = \text{argmax}\{m_j^T \hat{m}_j\}/F_S$ between ground-truth RF channels m_j and reconstructed channels $\hat{m}j$ were utilized as metrics for time-signal reconstruction quality. Additionally, a cost function $f_{cost} = \sum_r^R \left(SNR_{Yr}/\prod_c^{C_r} SNR_c\right)$ evaluates how effectively unipolar chipping sequences decorrelated RF channels, minimizing the signal-to-noise ratio (SNR) of the output from each multiplexr, while maximizing the SNR of the individual reconstructed RF channels.

Using the (locally-)optimal PRBS codes, results show the proposed method doubles the a-gCNR compared to classic TDM architectures at higher channel compression ratios (Fig.4b, d), enhancing contrast in anechoic regions. However, at an 8:1 compression ratio, both multiplexing methods exhibited significant loss of spatial precision below 2 mm (Fig.4d). As a result, the complete loss of information regarding the anechoic phantom with the smallest radius is observed, attributed to the use of a reduced (Nyquist) sampling rate during simulations [9].

The robustness of the proposed method relative to TDM was evaluated through simulations sweeping sampling frequency between $F_S \in [30, 60]$MHz $> 4 \times f_c$, and the channel compression ratio from 2:1 to 32:1 (Fig. 5). Optimal PRBS sequences were not used; instead, 10 simulation epochs were performed to obtain the CNR values presented in Fig. 5, averaging the CNR of each epoch. As expected, the proposed method showed no direct advantage over TDM at increased sampling rates while maintaining channel compression, once the energy recovered from each reconstructed channel converged to similar levels. However, by maintaining or reducing the sampling rate, the proposed method achieved up to 3.2 dB of additional CNR for the recovered B-mode images with increased channel compression compared to classical TDM.

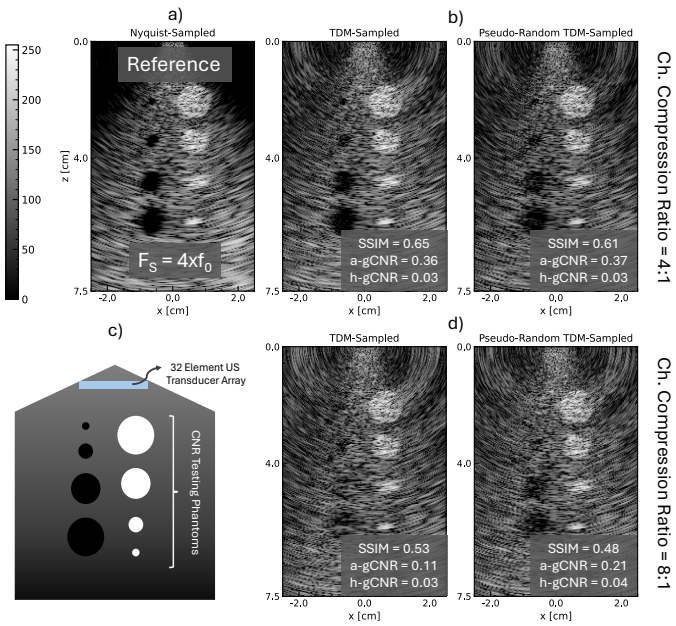

Fig. 4. PyMUST-simulated a) Reference B-mode image b) reconstructed B-mode images from TDM (left) and PRCS-TDM (right) architectures at a 4:1 Ch. compression ratio, c) Simulation media setup, d) reconstructed B-mode images from TDM (left) and PRCS-TDM (right) architectures at a 8:1 Ch. compression ratio.

VI. Conclusions

This study shows that under the same sampling rate, the PRCS-TDM architecture leveraging non-uniform sampling rates for each RF channel improves CNR over conventional TDM, enhancing the contrast of anechoic regions in B-mode images with up to double the a-gCNR, upon the increase of channel compression ratios (8:1). The contrast increase observed in anechoic regions is of special importance for US clinical applications targeting blood vessel-occupied regions. While PRCS-TDM does not outperform TDM at higher sampling frequencies, it offers up to 3.2 dB additional CNR at lower frequencies as channel compression ratio increases, highlighting its potential to improve image quality in AFE architectures with constraints on aspect ratio and power dissipation, thus providing a promising alternative to traditional TDM in next generation wearable and implantable USI ASICs.

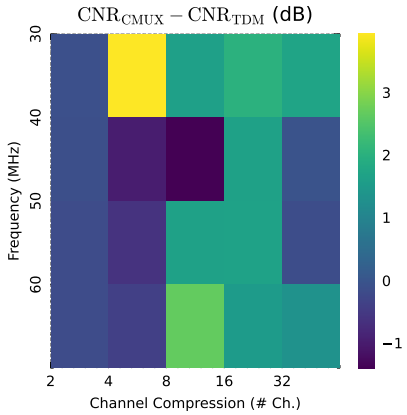

Fig. 5. Decibel CNR difference between PRCS-TDM and TDM for sweeping F_S and Ch. compression ratio.

REFERENCES

[1] Brönneke JB, Müller J, Mouratis K, Hagen J, Stern AD. Regulatory, Legal, and Market Aspects of Smart Wearables for Cardiac Monitoring. Sensors (Basel). 2021 Jul 20;21(14):4937. doi: 10.3390/s21144937. PMID: 34300680; PMCID: PMC8309890.

[2] C. Chen and M. A. P. Pertijs, "Integrated Transceivers for Emerging Medical Ultrasound Imaging Devices: A Review," in IEEE Open Journal of the Solid-State Circuits Society, vol. 1, pp. 104-114, 2021, doi: 10.1109/OJSSCS.2021.3115398.

[3] Y. M. Hopf et al., "A Pitch-Matched Transceiver ASIC With Shared Hybrid Beamforming ADC for High-Frame-Rate 3-D Intracardiac Echocardiography," in IEEE Journal of Solid-State Circuits, vol. 57, no. 11, pp. 3228-3242, Nov. 2022, doi: 10.1109/JSSC.2022.3201758.

[4] J.M. Rothberg, T.S. Ralston, A.G. Rothberg, J. Martin, J.S. Zahorian, S.A. Alie, N.J. Sanchez, K. Chen, C. Chen, K. Thiele, D. Grosjean, J. Yang, L. Bao, R. Schneider, S. Schaetz, C. Meyer, A. Neben, B. Ryan, J.R. Petrus, J. Lutsky, D. McMahill, G. Corteville, M.R. Hageman, L. Miller, & K.G. Fife,"Ultrasound-on-chip platform for medical imaging, analysis, and collective intelligence", Proc. Natl. Acad. Sci. U.S.A. 118 (27) e2019339118, https://doi.org/10.1073/pnas.2019339118 (2021).

[5] B. Lam, M. Price and A. P. Chandrakasan, "An ASIC for Energy-Scalable, Low-Power Digital Ultrasound Beamforming," 2016 IEEE International Workshop on Signal Processing Systems (SiPS), Dallas, TX, USA, 2016, pp. 57-62, doi: 10.1109/SiPS.2016.18.

[6] P. Guo et al., "A 1.2-mW/Channel Pitch-Matched Transceiver ASIC Employing a Boxcar-Integration-Based RX Micro-Beamformer for High-Resolution 3-D Ultrasound Imaging," in IEEE Journal of Solid-State Circuits, vol. 58, no. 9, pp. 2607-2618, Sept. 2023, doi: 10.1109/JSSC.2023.3271270.

[7] P. Guo et al., "A 125 μm-Pitch-Matched Transceiver ASIC With Micro-Beamforming ADC and Multi-Level Signaling for 3-D Transfontanelle Ultrasonography," in IEEE Journal of Solid-State Circuits, vol. 59, no. 8, pp. 2604-2617, Aug. 2024, doi: 10.1109/JSSC.2024.3355854.

[8] T. M. Carpenter, M. W. Rashid, M. Ghovanloo, D. M. J. Cowell, S. Freear and F. L. Degertekin, "Direct Digital Demultiplexing of Analog TDM Signals for Cable Reduction in Ultrasound Imaging Catheters," in IEEE Transactions on Ultrasonics, Ferroelectrics, and Frequency Control, vol. 63, no. 8, pp. 1078-1085, Aug. 2016, doi: 10.1109/TUFFC.2016.2557622.

[9] R. Tur, Y. C. Eldar and Z. Friedman, "Innovation Rate Sampling of Pulse Streams With Application to Ultrasound Imaging," in IEEE Transactions on Signal Processing, vol. 59, no. 4, pp. 1827-1842, April 2011, doi: 10.1109/TSP.2011.2105480.

[10] A. Besson, D. Perdios, M. Arditi, Y. Wiaux and J. -P. Thiran, "Compressive Multiplexing of Ultrasound Signals," 2018 IEEE International Ultrasonics Symposium (IUS), Kobe, Japan, 2018, pp. 1-4, doi: 10.1109/ULTSYM.2018.8580067.

[11] J. P. Slavinsky, J. N. Laska, M. A. Davenport and R. G. Baraniuk, "The compressive multiplexer for multi-channel compressive sensing," 2011 IEEE International Conference on Acoustics, Speech and Signal Processing (ICASSP), Prague, Czech Republic, 2011, pp. 3980-3983, doi: 10.1109/ICASSP.2011.5947224.

[12] Wang P, Jiang JY, Li N, Luo HW, Li F, Cui SG. Sparse dictionary for synthetic transmit aperture medical ultrasound imaging. J Acoust Soc Am. 2017 Jul;142(1):240. doi: 10.1121/1.4993644. PMID: 28764415; PMCID: PMC5513741.

[13] Yousufi M, Amir M, Javed U, Tayyib M, Abdullah S, Ullah H, Qureshi IM, Alimgeer KS, Akram MW, Khan KB. Application of Compressive Sensing to Ultrasound Images: A Review. Biomed Res Int. 2019 Nov 15;2019:7861651. doi: 10.1155/2019/7861651. PMID: 31828130; PMCID: PMC6885152.

[14] D. L. Donoho, "Compressed sensing," in IEEE Transactions on Information Theory, vol. 52, no. 4, pp. 1289-1306, April 2006, doi: 10.1109/TIT.2006.871582.

[15] J. A. Tropp, J. N. Laska, M. F. Duarte, J. K. Romberg and R. G. Baraniuk, "Beyond Nyquist: Efficient Sampling of Sparse Bandlimited Signals," in IEEE Transactions on Information Theory, vol. 56, no. 1, pp. 520-544, Jan. 2010, doi: 10.1109/TIT.2009.2034811.

[16] G. Bernardino and D. Garcia, "PyMUST: an open-Source Python Library for the Simulation and Analysis of Ultrasound," 2024 IEEE Ultrasonics, Ferroelectrics, and Frequency Control Joint Symposium (UFFC-JS), Taipei, Taiwan, 2024, pp. 1-4, doi: 10.1109/UFFC-JS60046.2024.10793881.

[17] G. Montaldo, M. Tanter, J. Bercoff, N. Benech and M. Fink, "Coherent plane-wave compounding for very high frame rate ultrasonography and transient elastography," in IEEE Transactions on Ultrasonics, Ferroelectrics, and Frequency Control, vol. 56, no. 3, pp. 489-506, March 2009, doi: 10.1109/TUFFC.2009.1067.

[18] H. Liebgott, A. Rodriguez-Molares, F. Cervenansky, J. A. Jensen and O. Bernard, "Plane-Wave Imaging Challenge in Medical Ultrasound," 2016 IEEE International Ultrasonics Symposium (IUS), Tours, France, 2016, pp. 1-4, doi: 10.1109/ULTSYM.2016.7728908.

[19] A. Rodriguez-Molares, O. M. Hoel Rindal, J. D'hooge, S. -E. Måsøy, A. Austeng and H. Torp, "The Generalized Contrast-to-Noise Ratio," 2018 IEEE International Ultrasonics Symposium (IUS), Kobe, Japan, 2018, pp. 1-4, doi: 10.1109/ULTSYM.2018.8580101.

[20] Zhou Wang, A. C. Bovik, H. R. Sheikh and E. P. Simoncelli, "Image quality assessment: from error visibility to structural similarity," in IEEE Transactions on Image Processing, vol. 13, no. 4, pp. 600-612, April 2004, doi: 10.1109/TIP.2003.819861.